



# A finite element analysis of thermoelastic damping in vented MEMS beam resonators



X. Guo<sup>a</sup>, Y.-B. Yi<sup>a,\*</sup>, S. Pourkamali<sup>b</sup>

<sup>a</sup> Department of Mechanical and Materials Engineering, University of Denver, U.S.A

<sup>b</sup> Department of Electrical Engineering, University of Texas at Dallas, U.S.A

## ARTICLE INFO

### Article history:

Received 21 February 2012

Received in revised form

5 April 2013

Accepted 25 April 2013

Available online 13 May 2013

### Keywords:

Thermoelastic damping

MEMS beam resonator

Finite element method

Eigenvalue method

Vents

## ABSTRACT

The effect of geometry on thermoelastic damping in micro-beam resonators is evaluated using an eigenvalue formulation and a customized finite element method. The vented clamped–clamped (CC) and clamped–free (CF) beams with square-shaped vents along their centerlines, are both analyzed by the finite element method. The quality factor and the resonant frequency are obtained as functions of various geometrical parameters including the location, number and size of the vents. The numerical results reveal that the addition of vent sections in the clamped end region can significantly increase the quality factor. The maximum improved quality factor as high as 3801 and 2257 times those of the CC and CF solid beams are realized. The methodology presented in this work provides a useful tool in design optimization of micro beam resonators against thermoelastic damping.

© 2013 Elsevier Ltd. All rights reserved.

## 1. Introduction

Microelectromechanical systems (MEMS) have been widely used as resonators for sensing [1–3] and electrical filtering [4–6] applications. One common type of resonators is a simple beam that can oscillate at its resonant frequency by electric actuation from an AC voltage source between the beam and the electrodes [7–9]. For design and fabrication of such a beam, one of the most important aspects is to achieve a high quality factor, as it is essential that the resonator vibrates consistently at the desired frequency and requires as little energy as possible to maintain its vibration. A higher quality factor is also preferred for signal selection.

There are many different mechanisms for energy dissipation inside micro-beam resonators, including thermoelastic damping, fluid damping [10–13], support loss [14] and surface loss [15–17]. Among these energy loss mechanisms, thermoelastic damping has been an active research area for a long term since it imposes an upper limit on the attainable quality factor. It arises from thermal currents generated due to contraction/expansion of elastic structures. The bending of micro-beams causes dilations of opposite signs on the upper and lower halves. Consequently, there is a transverse temperature gradient of finite thermal expansion in the structure, generating local heat currents. The mechanism was first explained by Zener [18,19] who named it internal friction for the

case of vibrating reeds. Zener also derived an approximate expression for thermoelastic damping, by keeping the first transverse thermal mode and neglecting the rest modes. Following this discovery, other scholars refined the theory via a number of different approaches. Lifshitz [20], for example, provided an exact solution to the linear thermoelastic equations in flexural-mode beam resonators. These analytical methods were later extended for other geometric structures. Wong [21,22] and Kim [23] presented mathematical expressions for thermoelastic damping in a ring gyroscope, based on Zener's and Lifshitz's method for flexural-mode rectangular beams, respectively. In a similar way, Sun [24] investigated the out-of-plane damping modes of circular plate resonators. Further, Hao [25] derived an exact solution for circular plates based on the thermal-energy approach, in which the generation of thermal energy per cycle of vibration was used in search of the solution of the quality factor. In addition to the analytical methods, the finite element formulation [26,27] was found a more efficient tool for those systems with complex geometrical shapes, mixed boundary conditions, or anisotropic material properties. Yi's group improved this method for beams, plates, axisymmetric rings [28] and derived a generalized eigenvalue scheme for the problems based on the Fourier reduction [29] in both two-dimensional and three-dimensional structures, even in the presence of fluid viscous damping [13]. In addition, the commercial software COMSOL<sup>®</sup> can be used for the problem, but the solution procedure requires the customer to provide the undamped frequency  $f_0$  at the beginning, and the numerical accuracy is dependent on the manual scaling settings [30].

\* Corresponding author. Tel.: +1 303 8712 228.

E-mail address: [Yun-Bo.Yi@du.edu](mailto:Yun-Bo.Yi@du.edu) (Y.-B. Yi).

However, limited research was performed on the practical methods to improve the quality factor by minimizing the damping loss. Candler et al.[31], for example, experimentally applied a specific addition to the geometry—slots cut in beams. The slots acted to disrupt heat flow across the beam, therefore altering the process of thermoelastic dissipation. This method enables tuning of the quality factor by structure design without the need to scale its size, thus allowing for enhanced design optimization. Inspired by this work, the current paper is seeking a predictive modeling tool that can be used to quantitatively evaluate the effect of beam geometry on the mitigation of thermoelastic damping. The methodology developed in this work is based on the eigenvalue finite element analysis of clamped–clamped (CC) and clamped-free (CF) beams with vents (slot cuts) along their centerlines. We aim for finding the optimal design of the geometry for maximizing the quality factor.

2. Methods

The schematic of a capacitive micro beam resonator [7] is shown in Fig. 1a along with the definitions of the relevant parameters. The driving force in the device is the Coulomb force of the capacity formed by the beam and the electrode. The micro beam is usually considered as a two-dimensional Euler–Bernoulli beam with a clamped–clamped boundary condition. The thermoelastic temperature mode of such a beam in its fundamental resonant frequency is shown in Fig. 1b. The heat flow induced by thermoelastic expansion and contraction is directed from the hot region to the cold region.

2.1. Analytical approach for thermoelastic damping

For a two-dimensional Euler–Bernoulli beam, the first governing equation [20] is formulated by adding the thermoelastic strain term to the equation of motion:

$$\rho A \frac{\partial^2 \mathbf{Y}}{\partial t^2} + \frac{\partial^2}{\partial x^2} \left( EI \frac{\partial^2 \mathbf{Y}}{\partial x^2} + E\alpha I_T \right) = 0 \tag{1}$$

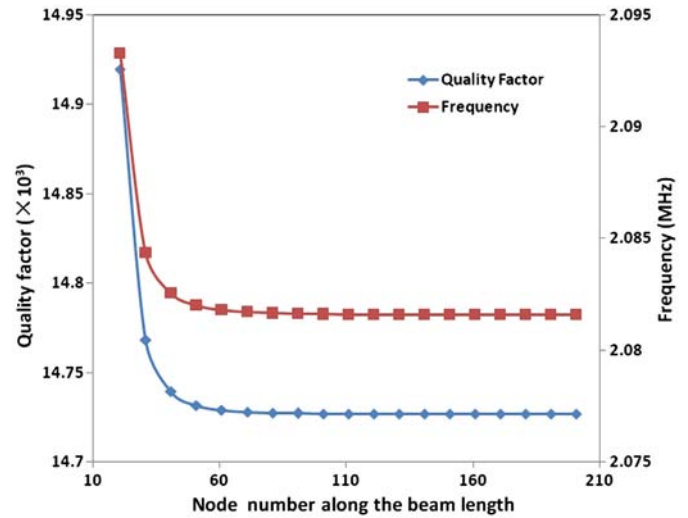


Fig. 2. A convergence study of the quality factor and resonant frequency.

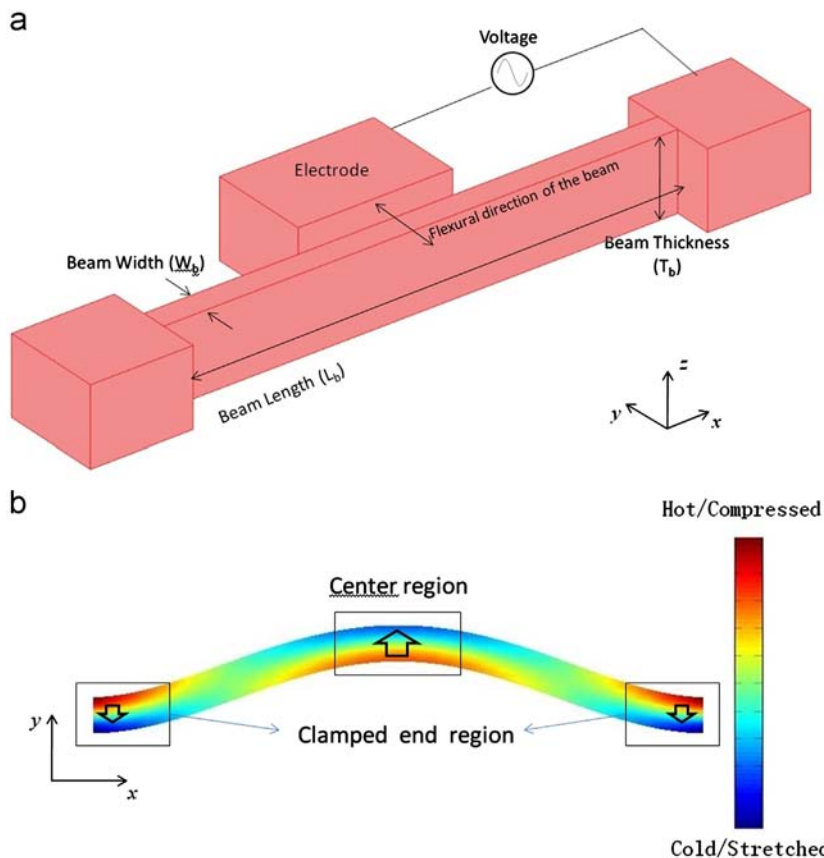


Fig. 1. (a) Schematic view of a clamped–clamped capacitive micro beam resonator. (b) Temperature contour plot of the clamped–clamped MEMS beam resonator in flexural vibration. The heat flow caused by the temperate gradient contributes to thermoelastic damping.

where  $x$  is the longitudinal position;  $Y$  is the out-of-plane displacement in the beam width as shown in Figs. 1 and 2;  $E$ ,  $\rho$  and  $\alpha$  are the elastic modulus, the density and the thermal expansion coefficient of the solid, respectively;  $A$  is the cross sectional area of the beam;  $I$  is the moment of inertia, and  $I_T$  defines the bending moment induced by the thermal deformation where

$$I_T = \int_A yTdydz \quad (2)$$

Note that the total temperature  $T_t$  is the sum of two parts  $T_t = T_0 + T$ , where  $T_0$  is the environment temperature and  $T$  is the fluctuating temperature caused by vibration. When the term  $E\alpha I_T$  is absent, Eq. (1) would degenerate to a free vibration without thermoelastic damping.

Similarly, the second coupling equation can be obtained by considering the heat generation caused by the alternating compression and stretching of the material. For the corresponding heat transfer problem, by neglecting the component of heat flux in the  $x$ -direction, the heat diffusion equation can be written in the following form:

$$\frac{\partial T}{\partial t} = k \frac{\partial^2 T}{\partial y^2} - \frac{E\alpha T_0}{(1-2\nu)c_v} \frac{\partial \varepsilon}{\partial t} \quad (3)$$

where  $k$ ,  $\nu$  and  $c_v$  are the thermal diffusivity, Poisson's ratio of the solid and the heat capacity of the solid, respectively;  $\varepsilon$  is the elastic strain. The last term in Eq. (3) is the heat generation due to thermal expansion/contraction.

Lifshitz's method [20] is a complex-frequency approach in which a harmonic motion is assumed in the perturbation form as follows:

$$Y(x, t) = Y_0(x)e^{i\omega t} \quad \text{and} \quad T(x, t) = T_0(x)e^{i\omega t} \quad (4)$$

where  $Y_0$  and  $T_0$  are the alternating amplitude of out plane displacement and the thermoelastic temperature, respectively. The temperature profile can be computed along the cross section of the beam by substituting Eq. (4) into Eq. (1). The obtained temperature profile can then be used to derive the mode of vibration that is defined as a complex value:

$$\omega = \text{Re}(\omega) + i\text{Im}(\omega) \quad \text{with} \quad i = \sqrt{-1} \quad (5)$$

where the real part  $\text{Re}(\omega)$  gives the new eigen-frequency of the beam in the present of thermoelastic damping while the imaginary part  $\text{Im}(\omega)$  indicates the attenuation in the vibration. The amount of thermoelastic damping, expressed in terms of the quality factor  $Q^{-1}$ , will then be determined by

$$Q^{-1} = 2 \left| \frac{\text{Im}(\omega)}{\text{Re}(\omega)} \right| \quad (6)$$

The final closed form solution [20] for thermoelastic damping is

$$Q^{-1} = \frac{E\alpha^2 T_0}{c_v} \left( \frac{6}{\xi^2} - \frac{6 \sinh \xi + \sin \xi}{\xi^2 \cosh \xi + \cos \xi} \right) \quad (7)$$

where

$$\xi = w \sqrt{\frac{\omega_0}{2k}} \quad (8)$$

The first undamped natural frequency  $\omega_0$  of the beam is

$$\omega_0 = \beta \sqrt{\frac{Ew^2}{12\rho L^4}} \quad (9)$$

where  $w$  is the width of the beam;  $L$  is the beam length and  $\beta$  is a coefficient determined by the boundary constraints. The value of  $\beta$  is 22.37 and 3.52 for clamped-clamped and clamped-free conditions, respectively [32].

## 2.2. Finite element formulation of thermoelastic damping

As stated in the previous section, a micro-beam can be simplified as either a two-dimensional plane strain or plane stress problem [33] to save the computational effort. Therefore, the following derivations are based on the two-dimensional problems only. The three-dimensional problems can be formulated in a similar way. The equation of motion written in the continuous form is

$$\rho \frac{\partial^2 \mathbf{u}}{\partial t^2} - \nabla(\mathbf{C}\mathbf{u} - \mathbf{D}\mathbf{T}) = \rho \ddot{\mathbf{u}} - \nabla(\mathbf{C}\mathbf{u} - \mathbf{D}\mathbf{T}) = 0 \quad (10)$$

$$\mathbf{C} = \frac{E}{(1+\nu)(1-2\nu)} \begin{bmatrix} 1-\nu & \nu & 0 \\ \nu & 1-\nu & 0 \\ 0 & 0 & 1/2-2\nu \end{bmatrix} \quad \text{for plane strain when } T_b > W_b \quad (11a)$$

$$\mathbf{C} = \frac{E}{1-\nu^2} \begin{bmatrix} 1 & \nu & 0 \\ \nu & 1 & 0 \\ 0 & 0 & (1-\nu)/2 \end{bmatrix} \quad \text{for plane stress when } T_b < W_b \quad (11b)$$

where  $\mathbf{u}$  is the displacement vector;  $\mathbf{T}$  is the alternating temperature;  $\mathbf{C}$  is the stiffness matrix;  $\mathbf{D}$  is the thermal expansion coefficient matrix;  $T_b$  and  $W_b$  are already explained in Fig. 1. The Galerkin finite element method is then applied to the single elemental domain to approximate the displacement field:

$$\mathbf{u} = [\mathbf{N}] \begin{bmatrix} \mathbf{u}_x & \mathbf{u}_y \end{bmatrix}^T = [\mathbf{N}] \{\mathbf{u}_e\} \quad (12)$$

$$\ddot{\mathbf{u}} = [\mathbf{N}] \begin{bmatrix} \ddot{\mathbf{u}}_x & \ddot{\mathbf{u}}_y \end{bmatrix}^T = [\mathbf{N}] \{\ddot{\mathbf{u}}_e\} \quad (13)$$

$$\mathbf{T} = [\mathbf{N}] \begin{bmatrix} \mathbf{T}_x & \mathbf{T}_y \end{bmatrix}^T = [\mathbf{N}] \{\mathbf{T}_e\} \quad (14)$$

$$\boldsymbol{\varepsilon} = \begin{bmatrix} \varepsilon_x & \varepsilon_y & \varepsilon_{xy} \end{bmatrix} = [\boldsymbol{\partial}] \mathbf{u} = ([\boldsymbol{\partial}][\mathbf{N}]) \{\mathbf{u}_e\} = [\mathbf{B}] \{\mathbf{u}_e\} \quad (15)$$

where  $\mathbf{N}$  is the shape function,  $\boldsymbol{\varepsilon}$  is the elastic strain tensor, the subscript  $e$  represents the elemental value. The Galerkin residual equation [34] in the entire physical domain is

$$\iint [\mathbf{N}]^T [\rho \ddot{\mathbf{u}} - \nabla(\mathbf{C}\mathbf{u} - \mathbf{D}\mathbf{T})] dx dy = 0 \quad (16)$$

Integration of the second and the third terms in Eq. (16) by parts yields

$$\begin{aligned} \iint [\mathbf{N}]^T \frac{\partial}{\partial x} (\mathbf{C}\boldsymbol{\varepsilon}) dx dy &= \iint [\mathbf{N}]^T [d(\mathbf{C}\boldsymbol{\varepsilon})] dy = - \iint [N, x]^T \mathbf{C}\boldsymbol{\varepsilon} dy \\ &+ \int [N]^T \mathbf{C}\boldsymbol{\varepsilon} dy \end{aligned} \quad (17)$$

$$\begin{aligned} \iint [\mathbf{N}]^T \frac{\partial}{\partial y} (\mathbf{C}\boldsymbol{\varepsilon}) dx dy &= \iint [\mathbf{N}]^T [d(\mathbf{C}\boldsymbol{\varepsilon})] dx = - \iint [N, y]^T \mathbf{C}\boldsymbol{\varepsilon} dx \\ &+ \int [N]^T \mathbf{C}\boldsymbol{\varepsilon} dx \end{aligned} \quad (18)$$

$$\begin{aligned} \iint [\mathbf{N}]^T \frac{\partial}{\partial x} (\mathbf{D}\mathbf{T}) dx dy &= \iint [\mathbf{N}]^T [d(\mathbf{D}\mathbf{T})] dy = - \iint [N, x]^T [d(\mathbf{D}\mathbf{T})] dy \\ &+ \int [N]^T \mathbf{D}\mathbf{T} dy \end{aligned} \quad (19)$$

$$\begin{aligned} \iint [\mathbf{N}]^T \frac{\partial}{\partial y} (\mathbf{D}\mathbf{T}) dx dy &= \iint [\mathbf{N}]^T [d(\mathbf{D}\mathbf{T})] dx = - \iint [N, y]^T [d(\mathbf{D}\mathbf{T})] dx \\ &+ \int [N]^T \mathbf{D}\mathbf{T} dx \end{aligned} \quad (20)$$

For free vibration, the boundary condition leads to

$$\int [N]^T C \epsilon dy = \int [N]^T C \epsilon dx = \int [N]^T D T dy = \int [N]^T D T dx = 0 \quad (21)$$

It follows

$$\iint [N]^T \rho [N] \{ \dot{\mathbf{u}}_e \} dx dy + \iint [B]^T C [B] \{ \mathbf{u}_e \} dx dy - \iint [N]^T D [N] \{ \mathbf{T}_e \} dx dy = 0 \quad (22)$$

Reducing this equation to the matrix form results in the following condensed expression:

$$M \{ \dot{\mathbf{u}}_e \} + L \{ \mathbf{u}_e \} - G \{ \mathbf{T}_e \} = 0 \quad (23)$$

**Table 1**

Silicon properties used in the analyses.

Young's modulus, $E$ (Pa)	$1.57 \times 10^{11}$
Poisson's ratio, $\nu$	0.22
Thermal expansion coefficient, $\alpha$ ( $K^{-1}$ )	$2.6 \times 10^{-6}$
Thermal conductivity, $k$ (W/mK)	90
Specific heat, $C_p$ (J/KgK)	700
Density, $\rho$ ( $kg/m^3$ )	2330
Temperature, $T_0$ (K)	300

**Table 2**

Convergence study.

Node number (length)	81	201	Error*
Quality factor	14,727.45	14,726.91	$3.667 \times 10^{-5}$
Frequency (Hz)	2,081,657	2,081,584	$3.507 \times 10^{-5}$

\* The error is estimated by comparing the result of 81 nodes with that of 201 nodes along the solid beam length.

where  $M$  is the mass matrix,  $L$  is the stiffness matrix and  $G$  is the thermal stress induced by thermal deformation.

Likewise, the governing heat diffusion equation, Eq. (3), in the differential form can be written as

$$k \nabla^2 T - \rho c_p \frac{\partial T}{\partial t} - C \frac{\partial \epsilon^*}{\partial t} = k \nabla^2 T - \rho c_p \dot{T} - C \dot{\epsilon}^* = 0 \quad (24)$$

For the plane strain condition, the strain rate that contributes to thermoelastic temperature only consists of two components  $\epsilon_x$  and  $\epsilon_y$ , because the shear strain  $\epsilon_{xy}$  does not generate any heat.

$$\dot{\epsilon}^* = \frac{\partial}{\partial t} (\epsilon_x + \epsilon_y) \quad (25)$$

The Galerkin finite element method is then applied to approximate the displacement and temperature fields as

$$\dot{\epsilon}^* = [N_x] \{ \dot{\mathbf{u}}_{ex} \} + [N_y] \{ \dot{\mathbf{u}}_{ey} \} = [B^*] \{ \dot{\mathbf{u}}_e \} \quad (26)$$

Compared with  $[B]$  in Eq. (15), the shear strain term is not included in the matrix  $[B^*]$ .

The Galerkin residual equation is

$$\iint [N]^T [k \nabla^2 T - \rho c_p \dot{T} - C \dot{\epsilon}^*] dx dy = 0 \quad (27)$$

Integration of the first term in Eq. (27) by parts yields

$$\begin{aligned} \iint [N]^T \frac{\partial}{\partial x} (k_x \mathbf{T}_{,x}) dx dy &= \iint [N]^T [d(k_x \mathbf{T}_{,x})] dy = - \iint [N_{,x}]^T k_x \mathbf{T}_{,x} dx dy \\ &+ \int [N]^T k_x \mathbf{T}_{,x} dy \end{aligned} \quad (28)$$

$$\begin{aligned} \iint [N]^T \frac{\partial}{\partial y} (k_y \mathbf{T}_{,y}) dx dy &= \iint [N]^T [d(k_y \mathbf{T}_{,y})] dx = - \iint [N_{,y}]^T k_y \mathbf{T}_{,y} dx dy \\ &+ \int [N]^T k_y \mathbf{T}_{,y} dx \end{aligned} \quad (29)$$

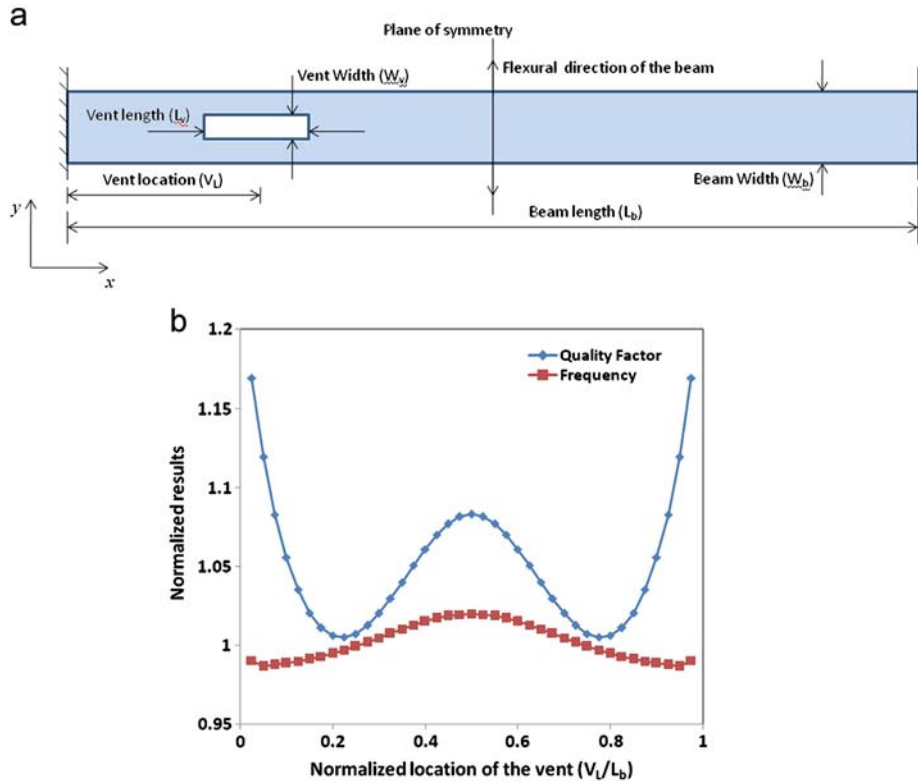


**Fig. 3.** (a) Schematic view of the beam resonator with a single vent. (b) Quality factor and frequency of the vented beam as functions of the vent location.

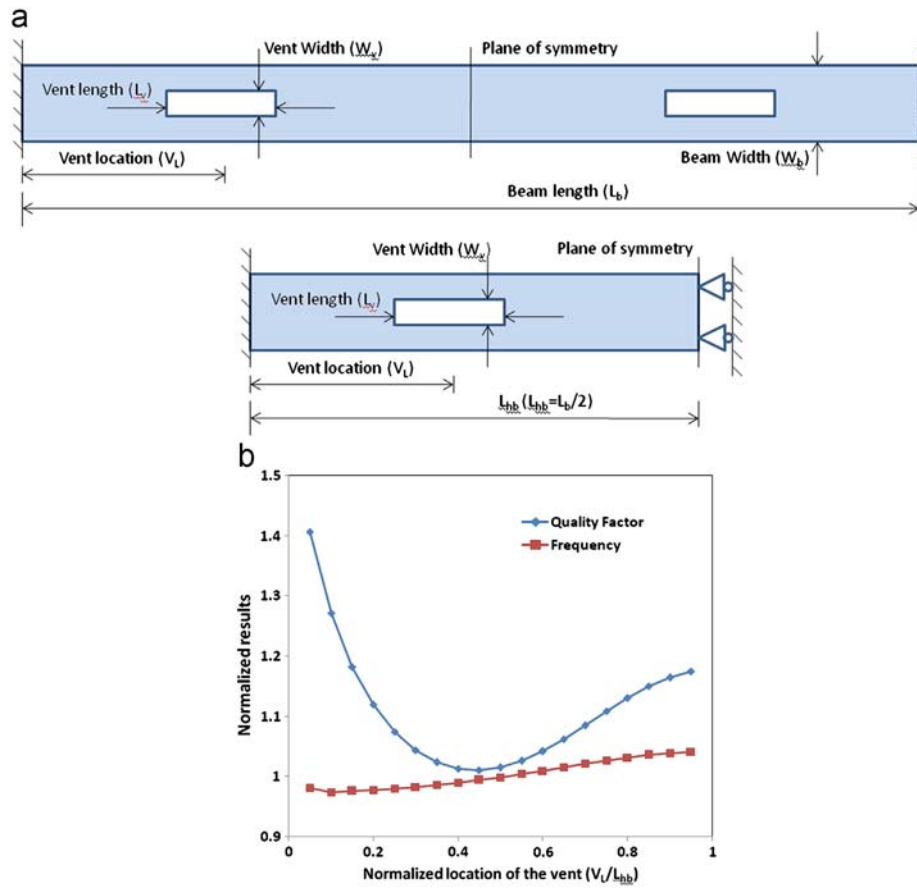


Fig. 4. (a) Schematic view of the beam with two symmetrically distributed vents. (b) Quality factor and frequency of the vented beam as functions of the vent locations.

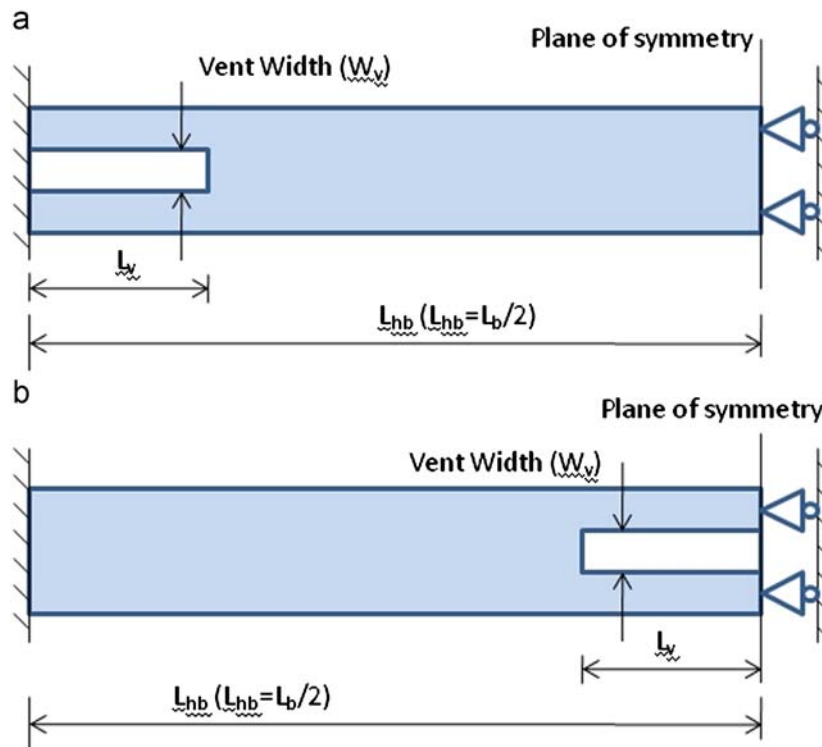


Fig. 5. Schematic view of a half beam resonator with two symmetrical vents located at (a) the clamped ends and (b) the beam center.

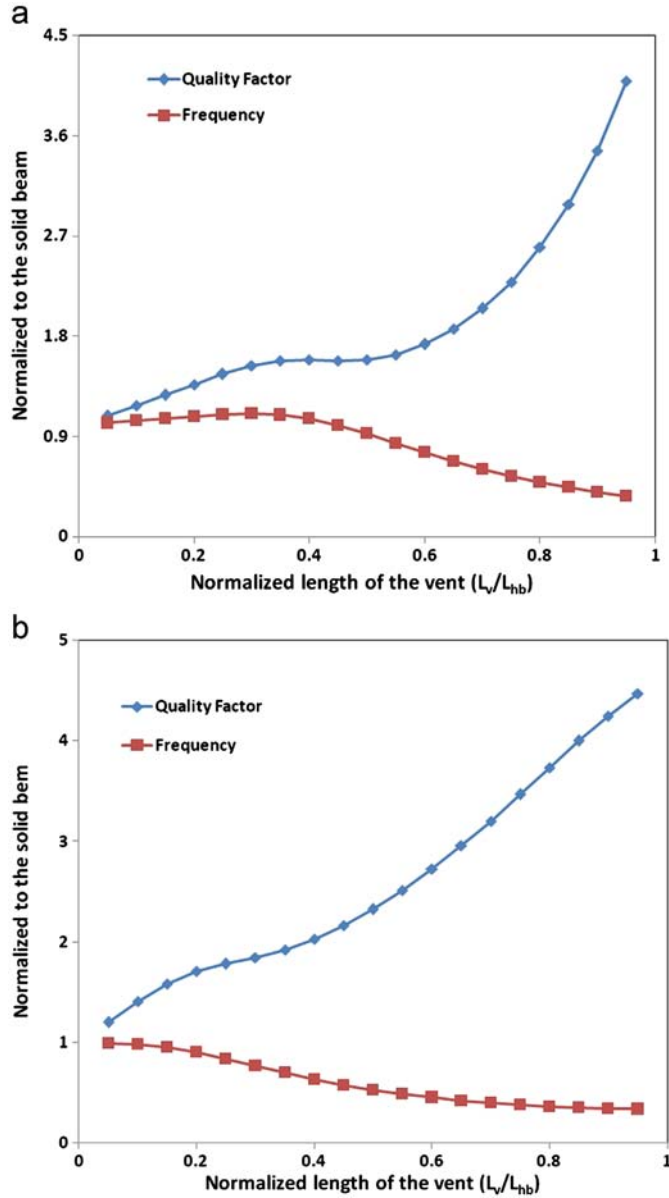


Fig. 6. Effects of the length of the symmetrical vents located at (a) the clamped end and (b) the beam center.

For the insulated thermal boundary condition, i.e.

$$\int [N]^T k_x \mathbf{T}_x dy = \int [N]^T k_y \mathbf{T}_y dx = 0 \quad (30)$$

It leads to

$$\iint [B]^T k [B] \{\mathbf{T}_e\} dx dy + \iint [N]^T \rho c_p [N] \{\dot{\mathbf{T}}_e\} dx dy + \iint [N]^T C [B^*] \{\dot{\mathbf{u}}_e\} dx dy = 0 \quad (31)$$

Rewriting this equation in the matrix form yields

$$K \{\mathbf{T}_e\} + H \{\dot{\mathbf{T}}_e\} + F \{\dot{\mathbf{u}}_e\} = 0 \quad (32)$$

where  $K$  is the thermal conductivity matrix,  $H$  is the heat generation matrix and  $F$  is the coupling matrix representing the heat generation induced by beam deformation. Similar to Eq.(4), here

we assume a perturbation form of the solution

$$\mathbf{T} = \mathbf{T}_0 e^{i\omega t} \quad (33)$$

$$\mathbf{u} = \mathbf{u}_0 e^{i\omega t} \quad (34)$$

$$\dot{\mathbf{u}} = \dot{\mathbf{u}}_0 e^{i\omega t} \quad (35)$$

It immediately follows that

$$\dot{\mathbf{u}} = \frac{\partial \mathbf{u}}{\partial t} = \frac{\partial}{\partial t} (\mathbf{u}_0 e^{i\omega t}) = i\omega (\mathbf{u}_0 e^{i\omega t}) = i\omega \mathbf{u} \quad (36)$$

$$\text{Substituting Eqs. (33)–(36) into Eqs. (23) and (32) results in} \\ i\omega M \{\dot{\mathbf{u}}_e\} + L \{\mathbf{u}_e\} - G \{\mathbf{T}_e\} = 0 \quad (37)$$

$$K \{\mathbf{T}_e\} + i\omega H \{\mathbf{T}_e\} + i\omega F \{\mathbf{u}_e\} = 0 \quad (38)$$

The final matrix equation by combining Eqs. (36)–(38) is

$$\begin{bmatrix} -K & 0 & 0 \\ G & -L & 0 \\ 0 & 0 & I \end{bmatrix} \begin{bmatrix} \mathbf{T}_e \\ \mathbf{u}_e \\ \dot{\mathbf{u}}_e \end{bmatrix} = i\omega \begin{bmatrix} H & F & 0 \\ 0 & 0 & M \\ 0 & I & 0 \end{bmatrix} \begin{bmatrix} \mathbf{T}_e \\ \mathbf{u}_e \\ \dot{\mathbf{u}}_e \end{bmatrix} \quad (39)$$

where  $i\omega$  is the eigenvalue of the equation.

The quality factor can then be obtained from Eq. (6). Since the energy dissipation of vibrating beams is mainly caused by thermoelastic heat generation and propagation, the quality factor can be improved by reducing the conduction path. We hypothesize that these goals can be achieved by adding vent sections to the solid beam to disrupt the heat flow across the thickness. To validate the hypothesis, the finite element method was applied to investigate the geometric effects on the quality factor and the resonant frequency with the presence of thermoelastic damping. For the micro-beam resonator shown in Fig. 1 whose thickness is greater than the width, the two-dimensional quadratic quadrilateral nine-node (Q9) plain strain elements were implemented in the model due to its higher precision than the four-node (Q4) elements. MATLAB<sup>®</sup> was used as the programming tool in the analysis.

### 3. Results and discussions

#### 3.1. Finite element convergence tests

To validate the method, the convergence tests were performed on a CC solid beam (without vents) of 200  $\mu\text{m}$  long ( $L_b$ ) and 10  $\mu\text{m}$  wide ( $W_b$ ). The beam was discretized into rectangular elements of the same size to ensure that the nodes were evenly distributed along both length and width. The node number along the length varied from 21 (i.e.10 elements) to 201 (i.e. 100 elements), while a fixed number of 7 nodes (i.e. 3 elements) was used in the width. The silicon material properties [28] are listed in Table 1. Poisson's ratio was set to zero for making a better comparison with the analytical results [20] that leave out the shear effect. The result of the convergence test is shown in Fig. 2. Compared to the analytical solution where the quality factor is 14,646 and the frequency is 2.11 MHz, the numerical error in the quality factor obtained by the finite element method is 0.55% by Q9 elements (14,747), meanwhile the error in the frequency is 1.42% by Q9 (2.08 MHz) correspondingly, when the maximum mesh density is used in the current analysis. It is also noticed that the convergent frequency is slightly lower than the analytical solution, because the latter is based on the Euler–Bernoulli beam model that is less accurate than the theory of elasticity. Fig. 2 also clearly indicates that the Q9 elements converge quickly to a fairly accurate solution when the node number along the length is greater than 81 (i.e. 40 elements). To balance the effort of computation and the accuracy, the results based on Q9 elements with two different mesh

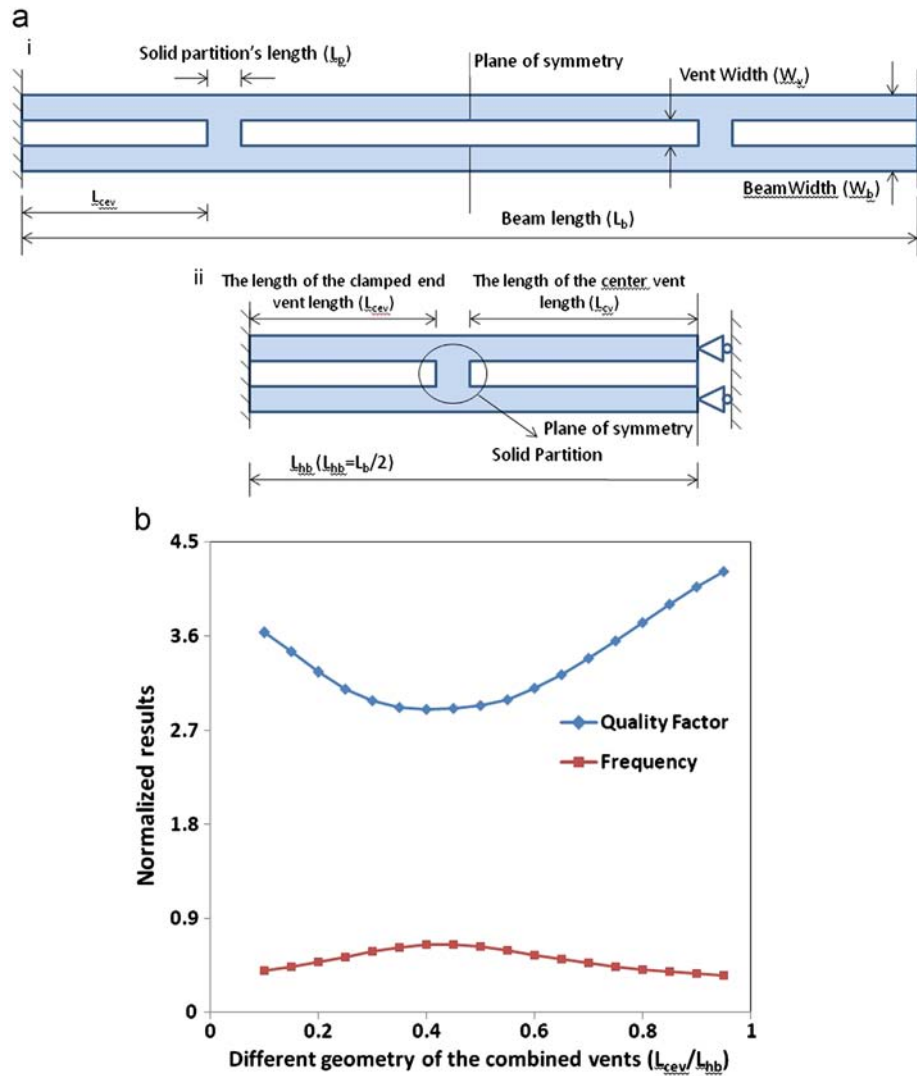


Fig. 7. (a) (i) Three-vent beam resonator and (ii) its corresponding half model; (b) Quality factor and frequency of the vented beam as functions of the vent length.

densities are compared in Table 2. The numerical accuracy shows that a  $7 \times 81$  mesh is sufficient for practical applications. When a realistic nonzero Poisson's ratio is taken into consideration, the quality factor and the frequency are 9400 and 2.13 MHz, respectively, based on the  $7 \times 81$  mesh.

### 3.2. The location of the vents

The same CC beams of  $200 \mu\text{m}$  long and  $10 \mu\text{m}$  wide are considered. The vented beam is shown in Fig. 3a (in the  $x$ - $y$  plane). To determine the optimal location of the vents, a single vent whose location varies along the beam with a fixed size,  $3.33 \mu\text{m}$  wide and  $10 \mu\text{m}$  long, has been studied. The vent location is defined by  $V_L$  that indicates the distance from the center of the vent to the left clamped end of the CC beam. The results of the quality factor and the frequency normalized against those of the solid beam are shown in Fig. 3b. The symmetry in the curves is caused by the symmetry in the vent locations with respect to the mid plane of the beam. The quality factor increases by 16.9% and the frequency increases by only 0.9% when the vents are located in the clamped region of the beam ( $V_L = L_b/2$ ). Another peak of the result appears when the vent is in the center region of the beam ( $V_L = L_b/2$ ). The quality factor is enhanced by 8.3% while the frequency is 2.0% higher than the solid beam. As

shown in Fig. 1b, the maximum temperature difference is generated in the clamped-end and the center of the solid beam. Therefore, a disruption of the heat flow path in these locations can increase the quality factor efficiently. By comparison, the vent located in the clamped end can improve the quality factor more efficiently than the center region.

Another set of analyses were performed on a beam with two vents located symmetrically with respect to the mid plane of the beam length, as shown in Fig. 4a. The size of a single vent remains the same as the previous section, i.e.  $3.33 \mu\text{m}$  wide and  $10 \mu\text{m}$  long. To improve the computational efficiency, the symmetry of the vented beam is utilized, as demonstrated in Fig. 4a. The results are shown in Fig. 4b. It has been found that the maximum increase in the quality factor is as much as 40.6% when both vents are located in the clamped ends of the CC beam, while the frequency is lowered by only 1.9%, in comparison with the solid beam. On the other hand, as the vents move to the center region ( $V_L = 95 \text{ mm}$ ) of the beam, the quality factor increases by 17.5%, while the frequency increases by 4.1%. The much higher quality factor for vents located in the clamped-ends compared to the beam center implies that thermoelastic damping in solid beams is predominantly contributed by the heat flow generated in the clamped-ends.

### 3.3. Geometric optimization of the vents - length

The vent size effects on the quality factor and the frequency are investigated for two vent locations: the clamped ends and the beam center, as illustrated in Fig. 5, since these locations lead to the maximum quality factors. The analysis of the length effect was performed by altering the beam length from 5  $\mu\text{m}$  to 95  $\mu\text{m}$  with a constant width of 3.33  $\mu\text{m}$ . The result is shown in Fig. 6. As expected, the quality factor increases with the vent length for both locations. In more detail, the quality factor increases almost linearly with the vent length when the vent is located in the clamped end. Meanwhile, for the vent located at the center, the increase in the quality factor is fairly slow at the beginning but gains its speed when the vent length approaches the beam length. The result of this comparison implies that the vents in the clamped ends can improve the quality factor more effectively than the vents in the beam middle. Fig. 6b shows that the frequency decreases when the vents are moving closer to the clamped end, since the presence of the vent section in the clamped end causes a

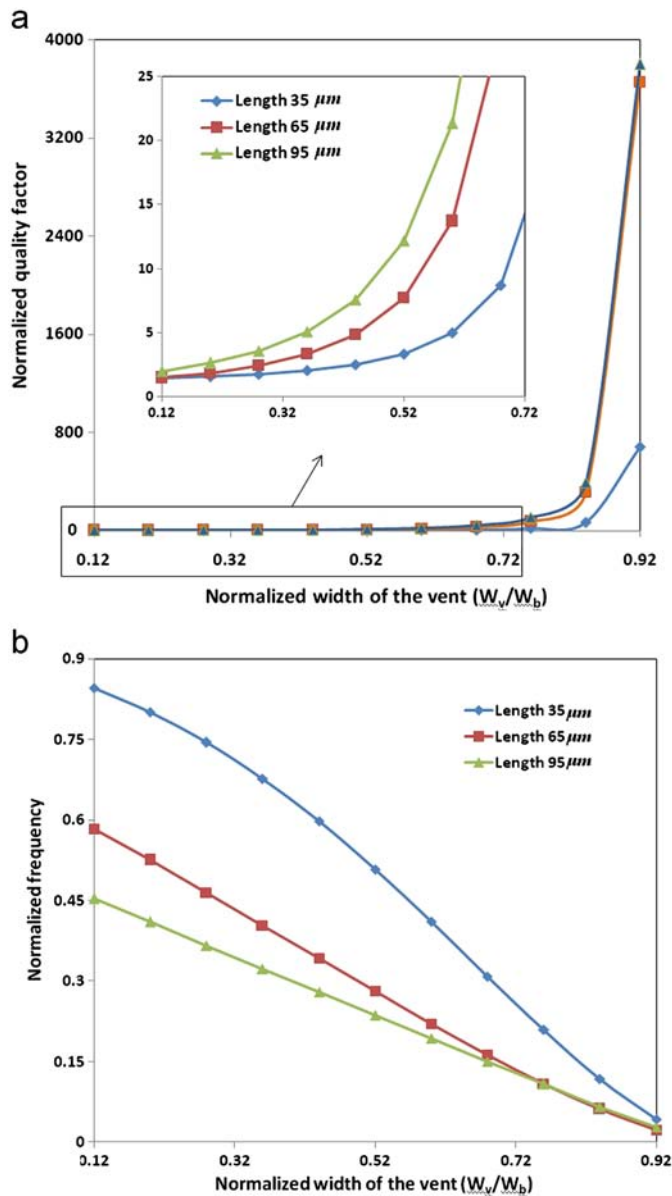


Fig. 8. (a) Quality factor and (b) Resonant frequency of the vented model as functions of the vent width and length, for vents symmetrically located at the clamped ends.

major loss of the structural stiffness. By implementing a vent of maximum length 95  $\mu\text{m}$  in present study, we have obtained a maximum increase in the quality factor as high as 347.3% while the frequency is lowered by 66.2% when the vents are located in the clamped ends. By comparison, the quality factor is raised by 308.9% and its frequency is reduced by 63.8% for the centered vents with the same length of 95  $\mu\text{m}$ .

In addition to the vents located in the clamped ends or the beam center, the effects of vents at other locations are also investigated. Fig. 7a shows a beam with three vents, each 3.33  $\mu\text{m}$  wide. The maximum full length of the vents is maintained as 95  $\mu\text{m}$  for consistency. The computational result is shown in Fig. 7b. It can be seen that the peak quality factor occurs when the vent at either location approaches its maximum length. In fact, the maximum increase in the quality factor is 322.1% corresponding to the longest vents located at the clamped ends. This result is higher than the maximum increase in the quality factor of the longest vents at the beam center, which is 263.9%. This demonstrates once again that the vents located at the clamped ends can improve the quality factor more efficiently than the vents located at the beam center. On the other hand, the change in the resonant frequency is opposite to that in the quality factor for the vented beam. Such a trend indicates that the vents in the clamped ends can reduce the structural rigidity of the system more significantly than other locations.

### 3.4. Geometric optimization of the vents—width

Based on the previous study, it has been shown that the highest quality factor can be achieved by symmetrically placing long vents in the clamped ends. In this section we focus on the investigation of the width effect as shown in Fig. 5a. The width of the vent is altered from 1.2  $\mu\text{m}$  to 9.2  $\mu\text{m}$  with different lengths of 35  $\mu\text{m}$ , 65  $\mu\text{m}$  and 95  $\mu\text{m}$ . The result in Fig. 8a indicates that vents of greater size (longer and wider) exhibit higher quality factors. For vents with constant length the quality factor increases sharply with the width. We also observed that the maximum quality factor of 65  $\mu\text{m}$ -long vents are slightly lower than 95  $\mu\text{m}$ -long vents but significantly higher than that of 35  $\mu\text{m}$ -long vents. It turns out that the highest achievable quality factor based on the present study is 3801 times that of the solid beam when the vent is 95  $\mu\text{m}$  long and 9.2  $\mu\text{m}$  wide. The change in the frequency is almost linear, as shown in Fig. 8b, meanwhile it converges to a much lower value as the width increases.

### 3.5. Geometric optimization of vented CF beam (cantilever)

By changing the boundary condition of the plane of symmetry in Fig. 5 to a free end, the CC beam becomes a clamped-free beam (CF or cantilever beam) with a half length. The contour plot of the temperature field in its fundamental resonant mode is shown in Fig. 9a. The greatest temperature variation takes place in the clamped end. Therefore, the optimal location of the vent to disrupt the heat flow is the clamped end. As a result a single vent in the clamped end of the cantilever beam is studied here. Vents with different lengths but a fixed width, 3.33  $\mu\text{m}$ , in the CF beam is analyzed and the results are presented in Fig. 9b. The quality factor increases quickly at the beginning but slows down when the vent length approaches the length of the entire beam. Such a trend is nearly opposite to the change in the clamped-clamped beam with the centered vents as shown in Fig. 6b. The quality factor increases by 586% and the resonant frequency is reduced by 49.8% when the vent reaches its maximum length of 95  $\mu\text{m}$  in the present work. On the other hand, investigations of the vent width in Fig. 9c and d shows similar trends compared to the CC beam. For the vented cantilever, the maximum quality factor achieved in this work is 2257 times that of the solid

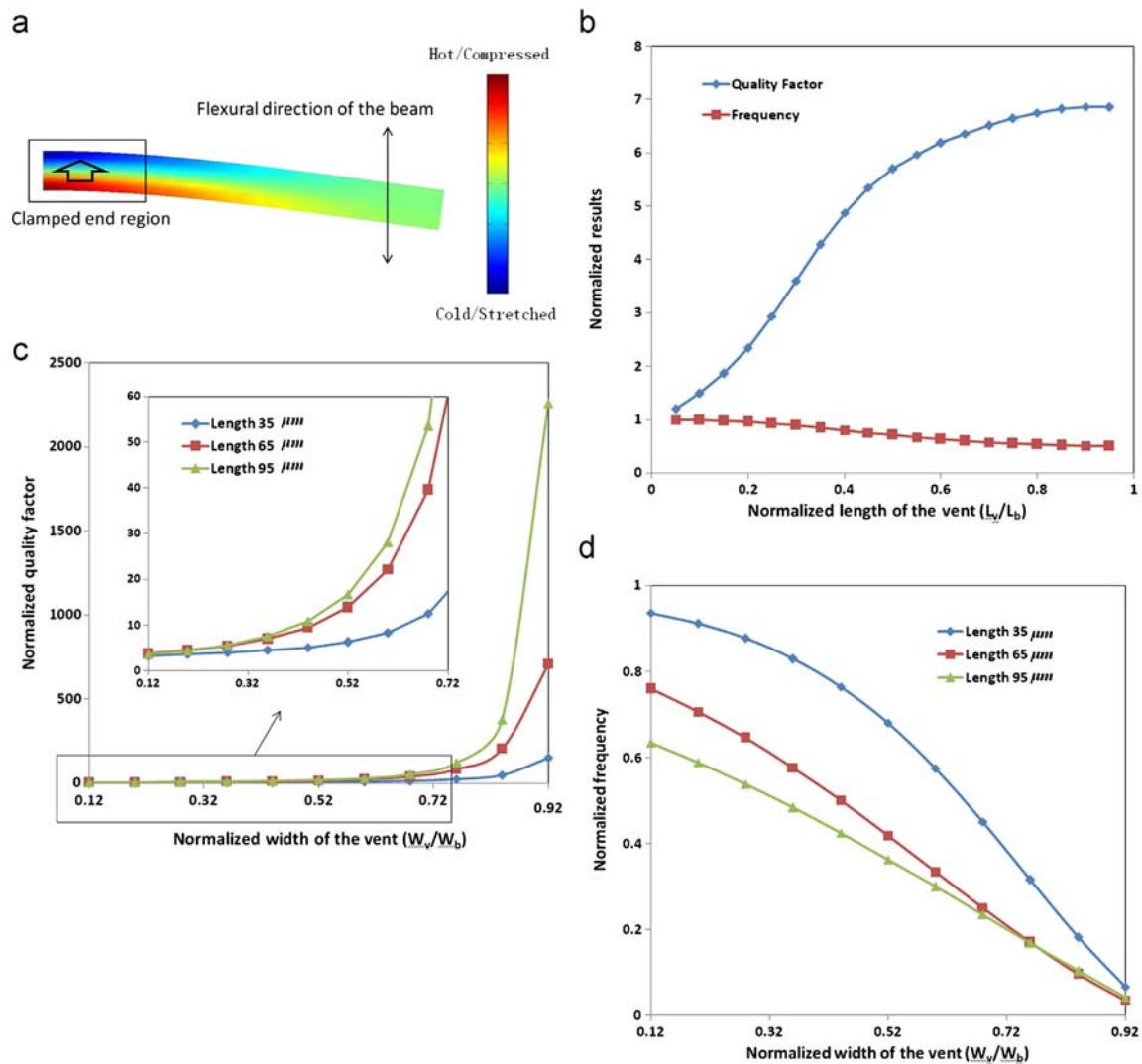


**Fig. 9.** (a) Temperature contour plot of the dominant flexural vibration mode of the clamped-free (CF) MEMS resonator; (b) The results of the CF beam with a vent at the clamped end as functions of the vent length; (c) The quality factor of the CF beam as a function of the vent width; (d) The resonant frequency of the CF beam as a function of the vent width.

cantilever when a vent section of  $95\ \mu\text{m}$  long and  $9.2\ \mu\text{m}$  wide is used.

#### 4. Conclusions

A customized finite element method is implemented on the MATLAB platform to investigate the geometric effects of vents on thermoelastic energy loss in clamped-clamped and clamped-free beam resonators. The quality factor and resonant frequency are obtained as functions of various geometric parameters including the location, number and size of the vents. For vented clamped-clamped beams, it has been found that the vents located in the clamped end and in the center region can both increase the quality factor very effectively compared to the other places, and the optimal location is found to be the clamped end. Although the quality factor can increase with the vent size, the effect of the vent width is typically more significant than the vent length. In the present study, the quality factor as high as 3801 times that of the solid beam has been achieved. On the other hand, the result shows that a vent located in the clamped end can reduce the structural rigidity and hence significantly reduce the resonant frequency. We

also investigated the effect of vents in a cantilever beam and similar conclusions have been obtained.

#### References

- [1] Zook D, Burns W, Herb R, Guckel H, Kang W, Ahn Y. Optically excited self-resonant micro beams. *Sensors Actuators* 1996;A52:92–8.
- [2] Evoy S, Carr DW, Sekaric L, Olkhovets A, Parpia JM, Craighead HG. Nanofabrication and electrostatic operation of single-crystal silicon paddle oscillations. *J Appl Phys* 1999;86:6072–7.
- [3] Lavrik NV, Sepaniak MJ, Datskos PG. Cantilever transducers as a platform for chemical and biological sensors. *Rev Sci Instrum* 2004;75:2229–53.
- [4] Wang K, Wong AC, Nguyen CT. VHF free-free beam high-Q micromechanical resonators. *J Microelectromech Syst* 2000;9(3):347–60.
- [5] Pourkamali S, Ayazi F. Electrically coupled MEMS bandpass filters-part I: with coupling element. *Sensors Actuators* 2005;A122:307–16.
- [6] Pourkamali S, Ayazi F. Electrically coupled MEMS bandpass filters-part II: without coupling element. *Sensors Actuators* 2005;A122:317–25.
- [7] Pourkamali S, Hashimura A, Ho GK, Erbil A, Ayazi F. High-Q single crystal silicon HARPSS capacitive beam resonators with self-aligned sub-100 nm transduction gaps. *J Microelectromech Syst* 2003;12:487–96.
- [8] Abdel-Rahman EM, Nayfeh AH. Secondary resonances of electrically actuated resonant microsensors. *J Micromech Microeng* 2003;13:491–501.
- [9] Nayfeh AH, Younis MI. Dynamics of MEMS resonators under superharmonic and subharmonic excitations. *J Micromech Microeng* 2005;15:1840–7.

- [10] Naik T, Longmire EK, Mantell SC. Dynamic response of a cantilever in liquid near a solid wall. *Sensors Actuators A: Phys* 2003;102:240–54.
- [11] De SK, Aluru NR. Coupling of hierarchical fluid models with electrostatic and mechanical models for the dynamic analysis of MEMS. *J Micromech Microeng* 2006;16:1705–19.
- [12] Basak S, Raman A, Garimella SV. Hydrodynamic loading of microcantilevers vibrating in viscous fluids. *J Appl Phys* 2006;99:114906.
- [13] Yi YB, Rahafrooz A, Pourkamali S. Modeling and testing of the collective effects of thermoelastic and fluid damping on silicon MEMS resonators. *J Micro/Nanolithogr MEMS MOEMS* 2009;08(02):023010.
- [14] Zamanian M, Khadem SE. Analysis of thermoelastic damping in microresonators by considering the stretching effect. *Int J Mech Sci* 2010;52:1366–75.
- [15] Muller P, Saul A. Elastic effects on surface physics. *Surface Sci Rep* 2004;54:157–258.
- [16] Gurtin ME, Murdoch AI. A continuum theory of elastic material surfaces. *Arch Ration Mech Anal* 1975;57:291–323.
- [17] Sheng H, Li H, Lu P, Xu H. Free vibration analysis for micro-structures used in MEMS considering surface effects. *J Sound Vib* 2010;329:236–46.
- [18] Zener C. Internal friction in solids: I. Theory of internal friction in reeds. *Phys Rev* 1937;52:230–5.
- [19] Zener C. Internal friction in solids: II. General theory of thermoelastic internal friction. *Phys Rev* 1937;53:90–9.
- [20] Lifshitz R, Roukes M. Thermoelastic damping in micro- and nanomechanical systems. *Phys Rev B* 2000;61:5600–9.
- [21] Wong SJ, Fox CHJ, McWilliam S, Fell CP, Eley RA. Preliminary investigation of thermo-elastic damping in silicon rings. *J Micromech Microeng* 2004;14:108–13.
- [22] Wong SJ, Fox CHJ, McWilliam S. Thermoelastic damping of the in-plane vibration of thin silicon rings. *J Sound Vib* 2006;293:266–85.
- [23] Kim SB, Na YH, Kim JH. Thermoelastic damping effect on in-extensional vibration of rotating thin ring. *J Sound Vib* 2010;329:1227–34.
- [24] Sun Y, Tohmyoh H. Thermoelastic damping of the axisymmetric vibration of circular plate resonators. *J Sound Vib* 2009;319:392–405.
- [25] Hao Z. Thermoelastic damping in the contour-mode vibrations of micro- and nano-electromechanical circular thin-plate resonators. *J Sound Vib* 2008;313:77–96.
- [26] Silver MJ, Peterson LD. Predictive elasto-thermodynamic damping in finite element models by using a perturbation formulation. *AIAA J* 2005;43:2646–53.
- [27] Segalman DJ. Calculation of damping matrices for linearly viscoelastic structure. *J Appl Mech* 1987;54:585–8.
- [28] Yi YB. Finite element analysis of thermoelastic damping in contour-mode vibrations of micro- and nanoscale ring, disk, and elliptical plate resonators. *ASME J Vib Acoust* 2010;132:1–7.
- [29] Yi YB. Geometric effects on thermoelastic damping in MEMS resonators. *J Sound Vib* 2008;309:588–99.
- [30] COMSOL Multiphysics 3.3 User's Manual. Los Angeles: COMSOL, Inc.; 2006.
- [31] Candler RN, Duwel A, Varghese M, Chandorkar SA, Hopcroft MA, Park WT, et al. Impact of geometry on thermoelastic dissipation in micromechanical resonant beams. *J Microelectromech Syst* 2006;15:927–34.
- [32] Thomson WT, Dahleh MD. *Theory of vibration with applications*. New Jersey: Prentice Hall; 1997.
- [33] Barber JR. *Elasticity*. The Netherlands: Kluwer Academic Publishers; 2002.
- [34] Cook RD, Malkus DS, Plesha ME, Witt RJ. *Concepts and applications of finite element analysis*. New York: John Wiley & Sons; 2007.